Journal of Power Sources 553 (2023) 232270

Contents lists available at ScienceDirect

Journal of Power Sources

journal homepage: www.elsevier.com/locate/jpowsour

Operando X-ray diffraction in transmission geometry « at home » from tape casted electrodes to all-solid-state battery

Kriti Choudhary [a,b], Ilda Olivia Santos Mendoza [a,b], Arina Nadeina [a,b], Dennis Becker [c], Tristan Lombard [a,b], Vincent Seznec [a,b], Jean-Noël Chotard [a,b,*]

[a] Université de Picardie Jules Verne, Laboratoire de Réactivité et Chimie des Solides (LRCS), 15 rue Baudelocque, 80000, Amiens, France
[b] Réseau sur le Stockage Electrochimique de l'Energie (RS2E), 15 rue Baudelocque, 80000, Amiens, France
[c] Bruker AXS GmbH, Oestliche Rheinbrueckenstr. 49, 76187, Karlsruhe, Germany

HIGHLIGHTS

- Operando X-ray diffraction in 20 s.
- Operando X-Ray diffraction of All-solid-State Batteries.
- Development of a new electrochemical cell in reflection or transmission geometry.

GRAPHICAL ABSTRACT

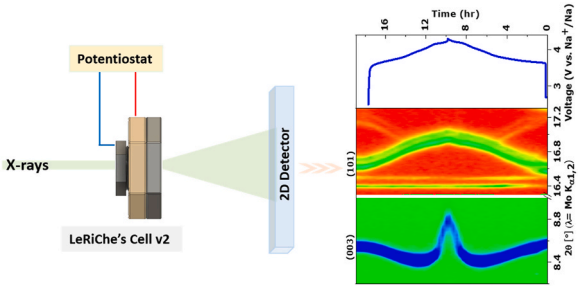

ARTICLE INFO

Keywords:
Operando X-ray diffraction
Operando electrochemical cell
All solid-state batteries
Li-ion batteries

ABSTRACT

The ever-growing field of energy storage needs the development of fast cycling rate and high energy density batteries and substantial research efforts are required to characterize them for improved performances. Operando X-ray diffraction is the most effective and convenient laboratory technique to get a deep insight into structural and electrochemical changes during operating conditions of batteries. In this work, we presented our newly developed operando LeRiChe'S Cell v2 which has been used to study NMC electrode materials not only with liquid electrolyte but also in solid-state batteries. The high brilliance of our laboratory diffractometer combined with our newly developed operando LeRiChe'S Cell v2 allowed us to investigate electrode materials at high C rates in a very short span of time.

1. Introduction

With the escalating demand for energy storage sources, all solid-state batteries (ASSB) have attracted attention because of their improved safety, wider operating temperature range, high energy densities and good stability compared to the liquid electrolyte-based batteries [1–4]. High cycling rate materials have also drawn extensive interests because they can provide more energy in a short span of time at low cost [5–7]. Efficient tools to properly characterize those systems in-depth are required to understand the mechanisms involved during the cycling of

* Corresponding author. Université de Picardie Jules Verne, Laboratoire de Réactivié et Chimie des solides (LRCS), 15 rue Baudelocque, 80000, Amiens, France.
E-mail address: jean-noel.chotard@u-picardie.fr (J.-N. Chotard).

https://doi.org/10.1016/j.jpowsour.2022.232270
Received 23 August 2022; Received in revised form 27 September 2022; Accepted 16 October 2022
Available online 25 October 2022

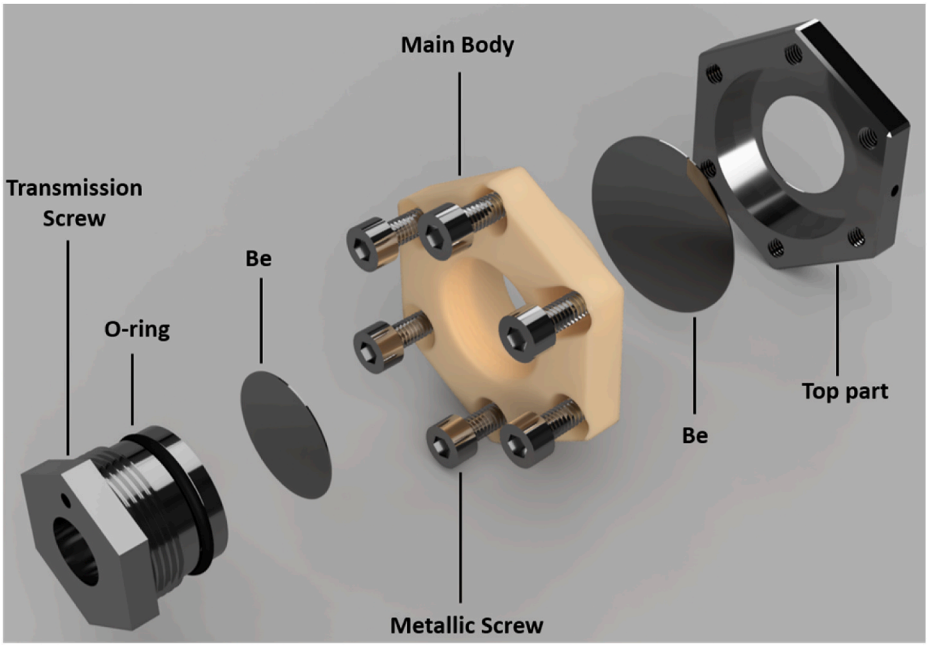

Fig. 1. Electrochemical Cell (LeRiChe'S Cell v2) designed for operando measurements in transmission geometry.

the batteries. The so-called operando measurements are therefore very crucial to unravel the correlation between electrochemical performances and structural changes of battery materials [8,9]. Many different operando characterization techniques such as Mössbauer Spectroscopy, Nuclear Magnetic Resonance (NMR), X-Ray Absorption Near Edge Spectroscopy (XANES), X-Ray Absorption Spectroscopy (XAS), Raman Spectroscopy, Electronic Microscopy (EM), Neutron and X-ray Diffraction methods (coherent and incoherent, elastic and inelastic) are being developed by different research teams all over the world [8,10–15].

Among them, operando X-Ray diffraction techniques are very likely the most spread characterization methods in research laboratories because of the easy use and adaptability of electrochemical cells into commercial diffractometers. The designing of a suitable and reliable operando electrochemical cell is the first and foremost part to ensure a successful operando XRD measurement. Imperfections in cell design can introduce many misleading and ambiguous results during operando measurements. Although there are several operando cells which have been designed and applied for XRD studies so far, there still exists scope for further innovation and development in the design of operando cells [16–22].

In this field, our laboratory has already demonstrated in the past its potential for innovation and ingenuity. Three electrochemical cells allowing concomitant measurements of electrochemical and structural properties have already been developed. The first one, is used in a powder diffractometer in reflection geometry [23]. The second version (called "LeRiChe'S Cell v1") developed in 2010 is dedicated to the synchrotron facilities, either for X-Ray diffraction or absorption measurement in transmission geometry [24]. Finally, a third cell adapted to neutron diffraction was developed in collaboration with ICMCB and ILL of Grenoble [25]. These different innovations have allowed us to reveal some intriguing reaction mechanisms within the electrode materials as well as to better understand the diffusivity of Li and/or Na in the batteries, as shown by recent experiments at the ALBA synchrotron [26]. Our quest to innovation further motivates us to redesign a new operando cell with improved efficiency to overcome every limitation encountered along the way of successful operando experiments.

One of the disadvantages of laboratory measurements is their slowness. Indeed, the current diffractometers (and in particular their detectors) allow to consider measurements of about 30 min in order to obtain a good counting statistic and *in fine* a diagram of sufficient quality to perform either a profile matching or a Rietveld refinement. Moreover, it is necessary to consider that during the X-Ray diffraction measurement, the stoichiometry of the active material will continue to evolve. Considering this, it is difficult to study materials at fast cycling rates (typically higher than C/20 or C/10).

Consequently, for studying materials at high cycling rates, the synchrotron remains the tool of choice since acquisitions of the order of 20 s are possible. Nevertheless, access to large-scale facilities is not always easy and yet it is absolutely necessary to be able to perform high quality and extremely fast operando measurements in the laboratory (in-house).

In this work, the synergetic development of i) a new operando cell adapted for both reflection and transmission geometry diffractometers and ii) the use of high brilliance and high energy (Molybdenum radiation) X-Ray source (rotating anode) is presented. This combination allows fast data collection (down to 20 s) as well as study of all solid-state batteries. An operating battery especially at fast charge and discharge rate is "out of equilibrium", therefore affecting the insertion and extraction mechanisms of electrode materials as a function of different *C*-rates. Thanks to this state-of-the-art diffractometer combined with our newly developed operando cell, we aim at studying "out of equilibrium processes" during cycling of high rate electrode materials.

2. Experimental

2.1. Operando cell development

The newly designed cell for carrying out operando measurements (called LeRiChe'S Cell v2) is schematized in Fig. 1. The top part of the cell is composed of stainless steel in a hexagonal shape with a hole of 1.7 cm in diameter. From the inner side of the top part, an X-Ray transparent window (either Beryllium, Aluminum or Glassy Carbon) can be placed. The transparent window also acts as a current collector and electrode material is analyzed directly by placing it over the window. The main body of the cell is made up of Polyether Ether Ketone (PEEK), which has excellent mechanical strength, high chemical and temperature resistance and provides good electrical insulation between the positive and the negative electrode [27]. This part of the cell contains a rubber O-ring to ensure a hermetic seal with the current collector window. The shape

of both main body and top part of the cell is hexagonal with similar dimensions and can be aligned very easily. Those two parts are put together through six metallic screws, which also act as connection points for the potentiostat. The important feature of this cell is the closing screw which is used to complete the assembling of the cell. There are two types of the closing screw one is reflection closing screw and the other is transmission closing screw. The operando LeRiChe'S Cell v2 can be used in transmission as well as in reflection geometry by simply exchanging the closing screw, which makes it easy to use, convenient and versatile. This characteristic feature makes LeRiChe'S Cell v2 unique, among all the operando XRD cell designed so far.

Also, thanks to the closing screw for applying sufficient stack pressure to the cell and keeping it air-tight for several weeks. This screw also has a small hole for electrical connection to the potentiostat with a 2 mm banana connector. The closing screws are made up of stainless steel with a rubber O-ring around the circumference which restrains electrolyte and air from escaping and entering the joining. In addition, the transmission screw has a cylindrical hole through it for transmission of X-rays and another O-ring in contact with another window (Be, or Al, or Glassy Carbon). Moreover, it also contains a spring for better electrical contact with current collector window. The newly designed operando LeriChe's Cell v2 is versatile, easy to assemble, light weight, compact, support good mechanical pressure and long lasting.

The LeRiChe'S Cell v2 is assembled by screwing the main body part (PEEK) of the cell with the top part. Then the active material is placed over the window followed by the separator which is soaked in electrolyte. Finally, the counter electrode is placed on the other side of the separator and the cell is tightened using the closing screw. As mentioned earlier, for transmission, another window of a smaller diameter is used and cell is tightened by using transmission screw. Obviously, for reflection geometry there is no need for extra x-ray transparent window. An aluminum or stainless-steel current collector can be used.

2.2. Rotating anode diffractometer

Operando measurements were performed on LeRiChe'S Cell v2 for both liquid and solid electrolyte containing $LiNi_{0.8}Mn_{0.1}Co_{0.1}O_2$ (NMC811) and $LiNi_{0.6}Mn_{0.2}Co_{0.2}O_2$ (NMC622) respectively in half-cell configuration. The diffractometer is a D8 DISCOVER from Bruker AXS, equipped with a rotating Mo anode (λ = 0.7093 Å) and a two-dimensional DECTRIS EIGER2R 500K detector. The beam has a flux density of 3×10^8 photons mm^{-2} sec^{-1} with a spot size at the sample (centre of the goniometer) of approximately 250 μm. The sample to detector distance is tuneable and has been set to 290.2 mm in order to cover an angular 2θ range of 6–21° in a single 2D snapshot (corresponding approximatively to 13–47° with Cu radiation). Rietveld Refinement was done using TOPAS software [28,29].

2.3. Electrochemical characterisation and electrodes preparations

Electrochemical characterization of all the electrode materials were performed using a VMP potentiostat from Biologic in half-cells configurations. The cells were cycled between 2.5 V and 4.3 V vs Li^+/Li at different C rates.

2.3.1. Liquid electrolyte cell assembly

Tape casted electrode of NMC811 from Umicore with 90 wt% of active material, 5 wt% conductive carbon, and 5 wt% PVDF were used for operando measurement. The electrodes had a porosity of ~32% and active material mass loading is 2.77 mg/cm^2. The LeRiChe'S Cell v2 was assembled in an Argon filled glove box, using the NMC811 electrode, two glass fiber separator, 300 μL liquid electrolyte (1 M $LiPF_6$ in 1:2% vol ethylene carbonate and diethylene carbonate, from Umicore) and lithium metal.

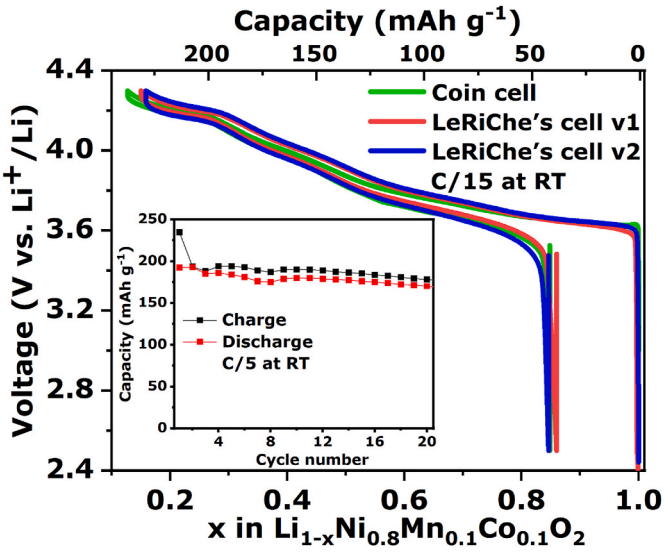

Fig. 2. Electrochemical cycle obtained with Coin cell, LeRiChe'S cell v1 and LeRiChe'S cell v2 at C/15. Inset represents the capacity retention at C/5 for 20 cycles done using LeRiChe's cell v2.

2.3.2. Solid electrolyte cell assembly

The cathode composite was prepared by using NMC622 and Li_6PS_5Cl (argyrodite) in weight ratio of 70:30. The solid electrolyte layer was composed of 100% Li_6PS_5Cl while a lithium metal foil was used as the negative electrode. First, the solid electrolyte was pressed at approximatively 100 MPa, using a conventional press and dye. Then, the solid-state battery pellet was assembled by pressing 34 mg of cathode composite with 328.5 mg of argyrodite and Li metal to about 375 MPa. The as-prepared stand-alone battery was finally introduced into the LeRiChe'S Cell v2 in between two glassy carbon windows to be used in transmission geometry. The cell was closed using a torque wrench (3.8 Nm) and kept as such during the whole measurement.

3. Results and discussion

3.1. Electrochemical tests

To test the reliability of the new operando cell, we performed the electrochemical characterization of Ni-rich NMC811 as cathode material using three different electrochemical cells: 1) a regular coin cell, 2) the first version of our electrochemical cell: LeRiChe'S cell v1 [24] and 3) our newly designed LeRiChe'S cell v2 (Fig. 2).

The electrodes were cycled at a rate of C/15 between 2.4 and 4.3 V vs Li^+/Li. The electrochemical voltage profiles for all of the three cells were relatively consistent. The LeRiChe'S Cell v2 designed for operando measurements showed reliable and comparable electrochemistry (with negligible polarization and comparable irreversibility) as obtained with other classical electrochemical cells. Longer measurements were also conducted in the LeRiChe'S Cell v2 in order to check the tightness of the cell. As it can be seen from the inset of Figs. 2 and 20 full cycles at C/5 were successfully measured for a total time of 200 h (i.e. more than 8 days).

3.2. Operando measurements in transmission geometry of batteries with liquid electrolyte

To study the characteristic changes in the materials' structure, operando XRD measurement has a significant importance. The reliability and efficiency of our laboratory X-ray (D8 Discover) was explored by studying the charge and discharge of NMC811 electrodes at different C rates and scan rates. Measurements were performed in transmission

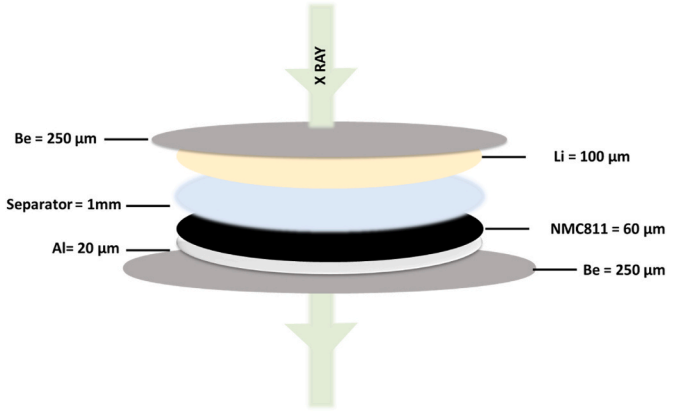

Fig. 3. Schematic view of the different layers crossed by the x-ray beam during the operando measurements.

geometry. The X-rays were transmitted through the whole LeRiChe'S Cell v2 composed of a stack of 6 different layers as shown in Fig. 3.

As mentioned above, the electrochemical measurements for charging and discharging of the operando cell were carried out between 4.3 and 2.5 V for the three different C rates. The operando NMC811/Li half cells were cycled at C/10, 1C, and 5C and the corresponding XRD patterns were recorded for 20 min/scan, 2 min/scan, and 20 s/scan respectively. The charge and discharge capacity of operando NMC811/Li half cells is 265 mAh g^{-1} and 214 mAh g^{-1} for C/10, 199 mAh g^{-1} and 180 mAh g^{-1} for 1C, and 137 mAh g^{-1} and 120 mAh g^{-1} for 5C respectively. The voltage curves for the three different C rates as a function of time is aligned with the diffraction patterns in Fig. 4. It is worth mentioning that even for data collected in 20 s, the reflections' intensities still allow to perfectly observe peak shift during cycling which is nearly impossible to analyze with common lab X-ray source. As observed previously by different groups [30–32], NMC811 undergoes structural changes from the pristine phase H1 to the isostructural phase H2 and finally into phase H3 isostructural to H1 and H2 if lithium content is less than 0.3. The (101) reflection is shifted towards higher 2θ continuously all along Li^+ deintercalation leading to a decrease in the *a* lattice parameter for all C rates. The (003) reflection is shifted first towards lower 2θ from 2.4 up to 4V and then towards higher 2θ at higher voltage upon Li^+ deintercalation for C/10 and 1C. Thus, the *c* lattice parameter is increased first before decreasing. A careful examination in the high voltage region (from 4.2 to 4.3 V) clearly shows a reversible bi-phasic mechanism. This trend has not been observed with a fast cycling rate of 5C. Indeed, only 0.65 lithium could be extracted from the pristine material while this bi-phasic behavior is observed only if more than 0.7 lithium are removed from the structure. The two constant peaks at 2θ value 16.39° and 16.49° identified by stars in Fig. 4, are associated with the Li metal used at anode.

The data quality collected in this experiment allow us not only to perform profile matching (as it is usually done with laboratory operando measurements) but to go one step further in doing Rietveld refinement. To do so, a dedicated macro was used in TOPAS [28,29] in order to consider, the absorption of the different layers of the battery as well as their individual relative displacement. From Rietveld refinement, evolution of *a* and *c* lattice parameters of NMC811 was studied for charge/discharge at different C rates. Fig. 5 illustrates the *a*-axis lattice parameters, *c*-axis lattice parameters and weight percentage of the H1, H2 and H3 phases as a function of x Li^+ in NMC811 for different C rates. It has been reported that at the end of charge a three-phase coexistence is observed at C/10 and 1C but not at 5C [30–32]. As explained above the amount of deintercalated Li^+ do not reach 0.7 and hence, the H3 phase does not appear. The existence of H1, H2 and H3 phases in NMC811 is

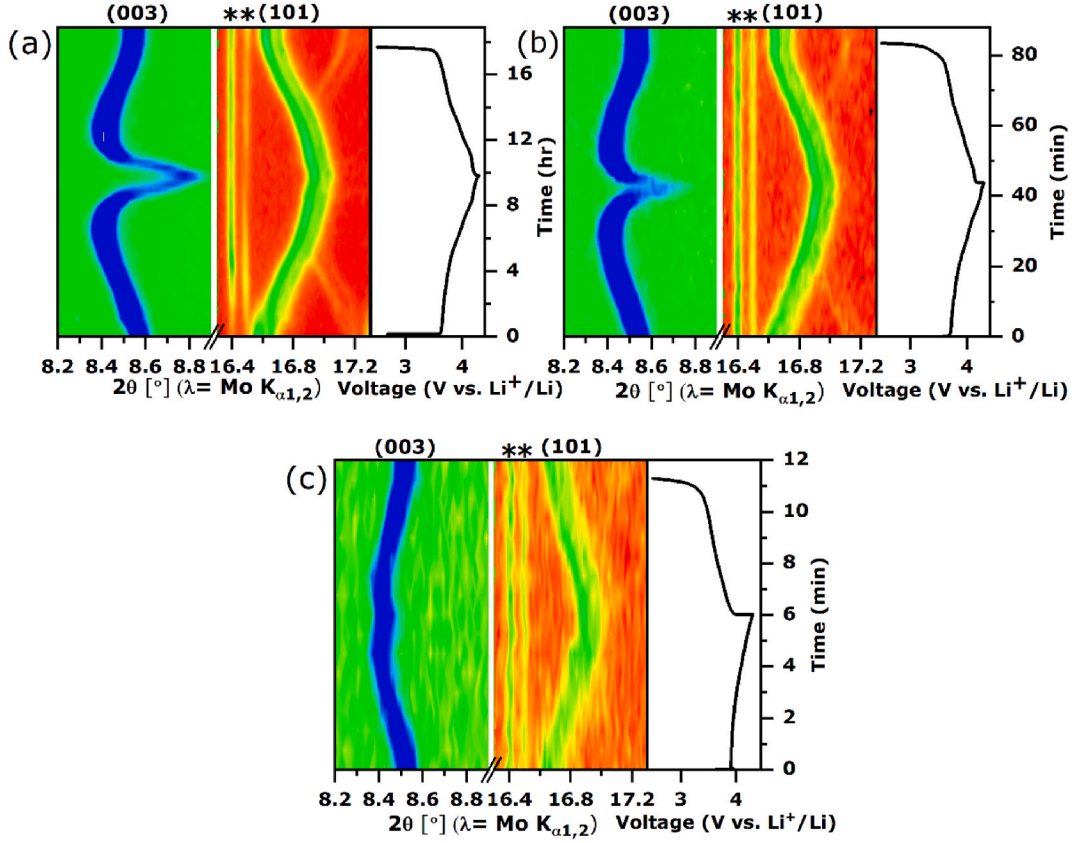

Fig. 4. Contour plots of operando XRD patterns of NMC811 for selected 2θ range at (a) C/10 for 20 min per scan (b) 1C for 2 min per scan and (c) 5C for 20 s per scan along with their electrochemical data. Peaks identified with a star correspond to Li metal.

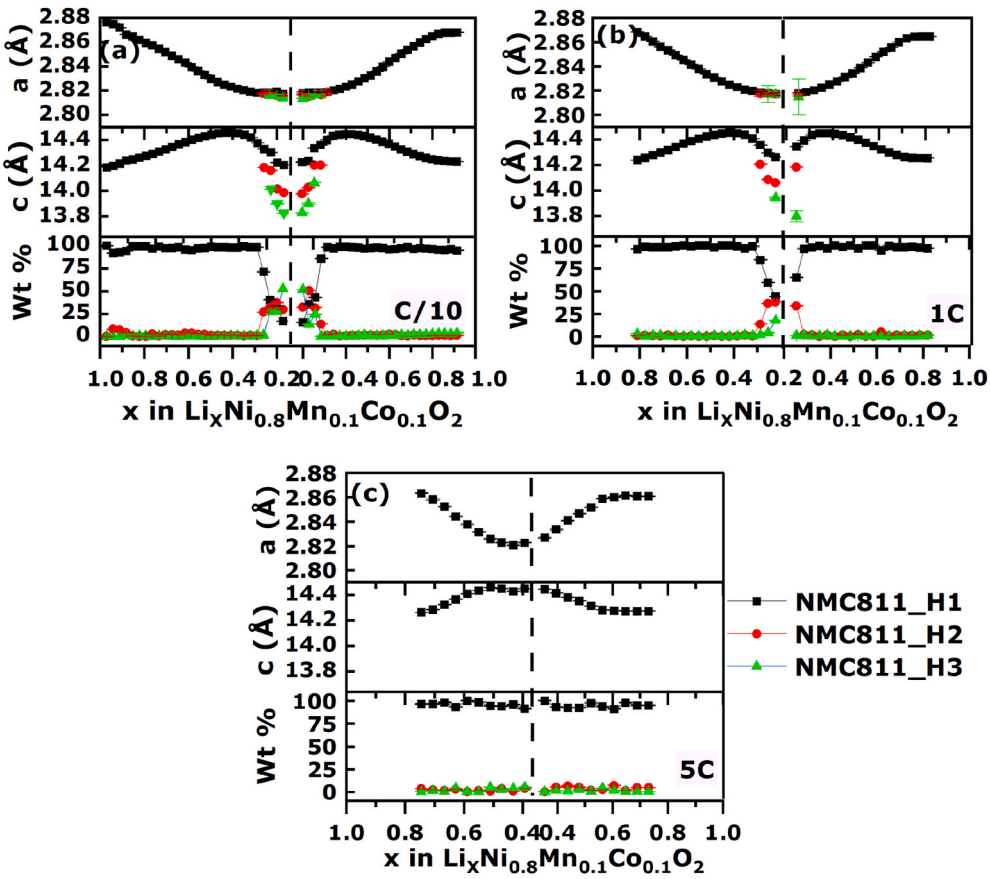

Fig. 5. Evolution of a and c lattice parameters and weight percentage of three phases of NMC811 (a) for C/10, (b) for 1C, and (c) for 5C during charge and discharge.

distinguished by black, red and green color markers. There is a continuous decrease in the *a* lattice parameter from 2.8765(2) Å to 2.8136(3) Å for C/10, 2.8681(2) Å to 2.817(2) Å for 1C, 2.8632(3) Å to 2.823(10) Å for 5C during charging. The value of the *a* lattice parameter shows a reversible behavior upon discharging with a gradual increase from 2.8133(3) Å to 2.8679(2) Å for C/10, 2.815(15) Å to 2.8646(2) Å for 1C, 2.8268(4) Å to 2.8608(3) Å for 5C. On the other hand, the *c* lattice parameter initially shows a continuous increase from 14.1840(5) Å to 14.4572(4) Å for C/10, 14.2377(6) Å to 14.4534(8) Å for 1C, 14.2609 (12) Å to 14.457(2) Å for 5C and then a rapid decrease only for C/10 and

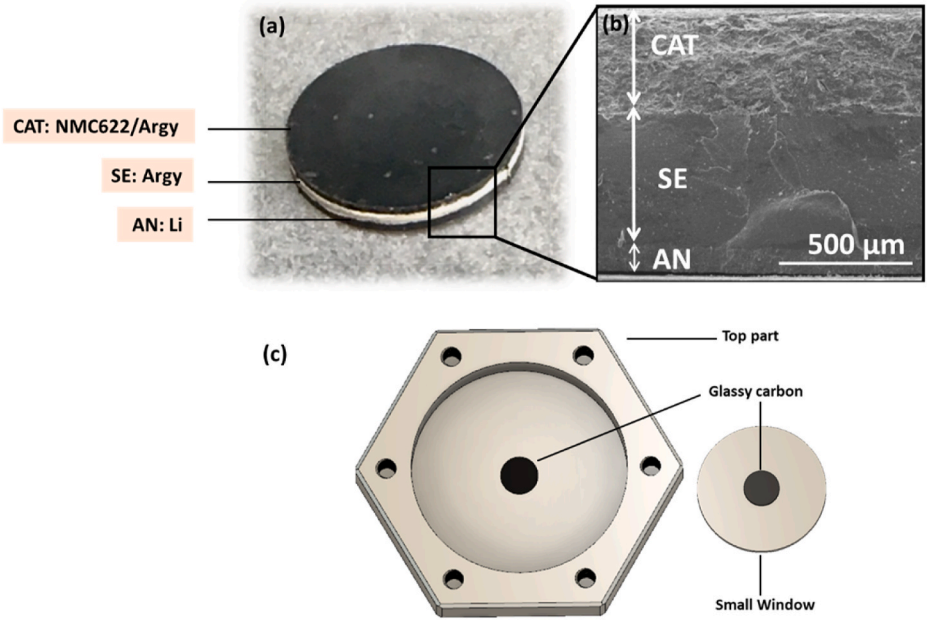

Fig. 6. Picture of (a) Composite electrode of NMC622/Argyrodite/Li ASSB and (b) its cross section by SEM and (c) top part and small window of LeRiChe'S Cell v2 with glassy carbon.

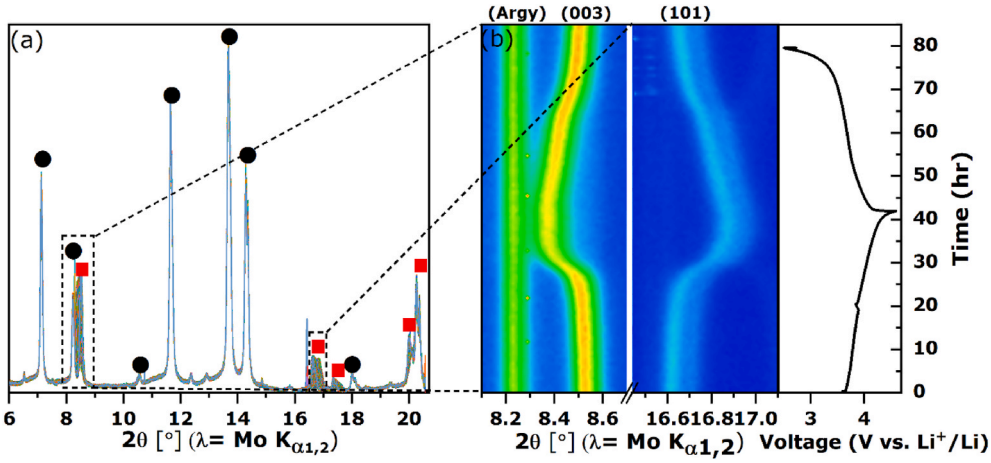

Fig. 7. (a) Operando XRD patterns of ASSB of NMC622/Argyrodite/Li, black circles correspond to the solid electrolyte phase (argyrodite) while the red squares correspond to the active material (NMC622) in the composite electrode (b) Contour plots of operando XRD patterns of NMC622/Argyrodite/Li cell at selected 2θ range. (For interpretation of the references to color in this figure legend, the reader is referred to the Web version of this article.)

1C upon charging and vice versa during discharging.

3.3. Operando measurements in transmission geometry of an all-solid-state-battery

All Solid-State Batteries (ASSB) are considered to be an alternative for replacing the flammable organic liquid electrolyte with the non-flammable solid electrolyte [33,34]. Li-argyrodite Li_6PS_5X (X = Cl, Br, I) is one of the promising solid electrolytes for solid-state batteries because of its high ionic conductivity, wide operating voltage and good electrochemical stability [35–37]. The operando X-Ray Diffraction measurements of NMC paired with Li-argyrodites can be very helpful to identify the structural and compositional changes, formation of solid solution, and reaction at electrode during battery cycling [38–40]. While operando techniques have been extensively studied in LIBs using liquid electrolyte, ASSB operando has received less attention, despite being so critical for future batteries [8,41,42]. The most important facets to study operando of solid-state batteries is the design of the operando cell. The availability of suitable operando cells which are air-tight, easy to assemble with reliable electrochemical cycling, and sufficient stack pressure to explore the batteries using solid electrolyte is very limited as compared to conventional batteries using liquid electrolyte [43–45]. The pressure which is applied to assemble the operando cell has a significant role in performance of solid-state batteries because of the contact between the cell and battery stack.

The use of standard large beryllium or glassy carbon windows are not suitable for this purpose as they can either bend or break with the applied high pressure. So, we have developed a dedicated "top part" and "small window" for our newly designed cell into which a glassy carbon disc (diameter = 5 mm; thickness = 250 μm) can be fit easily (Fig. 6 (c)). With this setup, we could close the cell using a torque of 3.8 Nm without breaking the windows and deforming the "top part" of the cell.

Our operando LeRiChe'S Cell v2 helped us to investigate the structural evolution of NMC622 during the charge and discharge process. An all solid-state NMC622/Li_6PS_5Cl/Li was assembled in LeRiChe'S Cell v2 as detailed in the experimental part. Fig. 6 (a,b) shows the picture of a typical three-layered solid-state battery along with its corresponding cross-section by scanning electron microscopic image. The total thickness of the battery was around 1000 μm. The three-layer pellet was then placed between two glassy carbon windows and the assembled cell was connected to a potentiostat. The electrochemical measurements for charging and discharging of NMC622/Argyrodite/Li operando cell were carried out between 2.4 and 4.6 V at C/60 rate at room temperature; the X-ray diffraction patterns were recorded after every 10 min during cycling. Fig. 7(a) shows the operando X-ray diffraction data of an ASSB NMC622/Argyrodite/Li in transmission mode. The galvanostatic data revealed that the ASSB delivers a charge and discharge capacity of 113 mAh g^{-1} and 104 mAh g^{-1} respectively. This is approximatively half of the practical capacity reached with the classical liquid-based electrolyte LIB [32,46,47]. We attribute this difference to the applied pressure which is lower in the LeRiChe'S cell v2 compare to what can be achieve in classical electrochemical cell. Nevertheless, the high energy X-ray beam was able to go through the whole cell and the powder data were successfully recorded. The fixed diffraction peaks marked with a black circle correspond to the solid electrolyte phase (argyrodite) while the red square correspond to the positive electrode (NMC622). The voltage curve with time is shown in Fig. 7(b) along with two-dimensional contour plot of selected two theta XRD scans. The significant shifts in Bragg peaks have been observed corresponding to the expansion and contraction of *c* and *a* lattice parameters of the NMC622. It has been also observed that the argyrodite peaks remain unaltered, meaning that the solid electrolyte was stable throughout the operando experiment from the diffraction point of view.

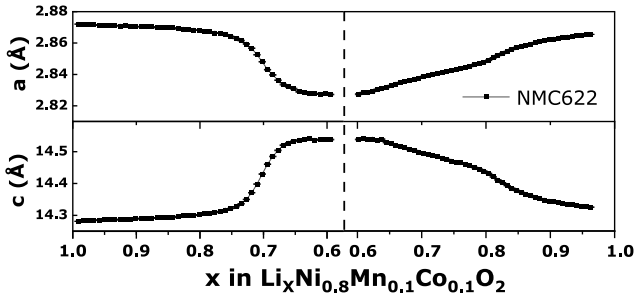

Fig. 8. Evolution of a and c lattice parameters of NMC622 at C/60 during charge and discharge.

Rietveld refinement was also performed for ASSB of NMC622/Argyrodite/Li. Fig. 8 shows the *a*-axis lattice parameters and *c*-axis lattice parameters as a function of x Li^+ in NMC622. The *a* lattice parameter decreases continuously from 2.8721(2) Å to 2.8272(2) Å upon charging and increases from 2.8274(3) Å to 2.8655(2) Å during discharging. On the other hand, *c* lattice parameter increases from 14.2813 (6) Å to 14.5380(11) Å upon charging and decreases from 14.5383(12) Å to 14.3257(7) Å during discharging. Therefore, our newly developed electrochemical operando LeRiChe'S Cell v2 is well suited for laboratory

X-ray diffraction of not only liquid but also solid-state batteries.

4. Conclusions

To understand those mechanisms, and consequently improve the batteries performances, it is crucial to investigate the reaction paths upon fast cycling. Our newly designed operando LeRiChe'S Cell v2 combined with a high flux x-ray source demonstrated that it is indeed possible to run very fast measurements "at home" (down to 20 s of collection time per pattern). The mechanisms involved at low or fast cycling rates can be observed, identified and analyzed through Rietveld refinements. Finally, the high penetration power of the Molybdenum rotating anode diffractometer allowed us to study full solid-state batteries and structural evolution of the active material in the composite electrodes upon cycling. In addition, we expect to see the possible phases formation at the interface between the electrolyte and the active material.

Author staement

Kriti Choudhary: performed the experiments, drafted the original manuscript, Dennis Becker: performed the Rietveld refinements, Arina Nadeina: performed the experiment on All Solid State Batteries, Ilda Olivia Santos Mendoza: prepared the electrodes materials, Tristan Lombard: assembled the All Solid State Batteries, Vincent Seznec: performed the x-ray acquisition, drafted the original manuscript, Jean-Noël Chotard: performed the x-ray acquisition, drafted the original manuscript, All authors have discussed the results and given approval to the manuscript.

Declaration of competing interest

The authors declare that they have no known competing financial interests or personal relationships that could have appeared to influence the work reported in this paper.

Data availability

Data will be made available on request.

Acknowledgements

This work was supported by the DESTINY Marie Sklodowska-Curie COFUND PhD Programme (Grant Agreement #945357) co-funded by European Commission. The rotating anode diffractometer was purchased with the support of the European Regional Development Fund (ERDF), the CNRS and Région Hauts-de-France (CPER grant #18001834). We are thankful to Umicore for providing us electrolyte and electrode materials.

References

[1] K. Takada, Progress and prospective of solid-state lithium batteries, Acta Mater. 61 (2013) 759–770.
[2] Y. Kato, S. Hori, T. Saito, K. Suzuki, M. Hirayama, A. Mitsui, M. Yonemura, H. Iba, R. Kanno, High-power all-solid-state batteries using sulfide superionic conductors, Nat. Energy 1 (2016) 1–7.
[3] C. Sun, J. Liu, Y. Gong, D.P. Wilkinson, J. Zhang, Recent advances in all-solid-state rechargeable lithium batteries, Nano Energy 33 (2017) 363–386.
[4] M. Pasta, D. Armstrong, Z.L. Brown, J. Bu, M.R. Castell, P. Chen, A. Cocks, S. A. Corr, E.J. Cussen, E. Darnbrough, V. Deshpande, C. Doerrer, M.S. Dyer, H. E. Shinawi, N. Fleck, P. Grant, G.L. Gregory, C. Grovenor, L.J. Hardwick, J.T. S. Irvine, H.J. Lee, G. Li, E. Liberti, I. McClelland, C. Monroe, P.D. Nellist, P. R. Shearing, E. Shoko, W. Song, D.S. Jolly, C.I. Thomas, S.J. Turrell, M. Vestli, C. K. Williams, Y. Zhou, P.G. Bruce, Journal of Physics : energy 2020 roadmap on solid-state batteries, J. Phys. Energy 2 (2020), 32008.
[5] B. Kang, G. Ceder, Battery materials for ultrafast charging and discharging, Nature 458 (2009) 190–193.
[6] G.L. Zhu, C.Z. Zhao, J.Q. Huang, C. He, J. Zhang, S. Chen, L. Xu, H. Yuan, Q. Zhang, Fast charging lithium batteries: recent progress and future prospects, Small 15 (2019) 1–14.
[7] M. Weiss, R. Ruess, J. Kasnatscheew, Y. Levartovsky, N.R. Levy, P. Minnmann, L. Stolz, T. Waldmann, M.W. Mehrens, D. Aurbach, M. Winter, Y.E. Eli, J. Janek, Fast charging of lithium-ion batteries: a review of materials aspects, Adv. Energy Mater. 11 (2021).
[8] F. Strauss, D. Kitsche, Y. Ma, J.H. Teo, D. Goonetilleke, J. Janek, M. Bianchini, T. Brezesinski, Operando characterization techniques for all-solid-state lithium-ion batteries, Adv. Energy Sustain. Res. 2 (2021), 2100004.
[9] D. Liu, Z. Shadike, R. Lin, K. Qian, H. Li, K. Li, S. Wang, Q. Yu, M. Liu, S. Ganapathy, X. Qin, Q.H. Yang, M. Wagemaker, F. Kang, X.Q. Yang, B. Li, Review of recent development of in situ/operando characterization techniques for lithium battery research, Adv. Mater. 31 (2019) 1–57.
[10] L. Aldon, A. Perea, M. Womes, C.M. Ionica-Bousquet, J.C. Jumas, Determination of the Lamb-Mössbauer factors of LiFePO4 and FePO4 for electrochemical in situ and operando measurements in Li-ion batteries, J. Solid State Chem. 183 (2010) 218–222.
[11] K. Märker, C. Xu, C.P. Grey, Operando NMR of nmc811/graphite lithium-ion batteries: structure, dynamics, and lithium metal deposition, J. Am. Chem. Soc. 142 (2020) 17447–17456.
[12] J. Wandt, A. Freiberg, R. Thomas, Y. Gorlin, A. Siebel, R. Jung, H.A. Gasteigera, M. Trompc, Transition metal dissolution and deposition in Li-ion batteries investigated by operando X-ray absorption spectroscopy, J. Mater. Chem. 4 (2016) 18300–18305.
[13] J. Fawdon, J. Ihli, F. La Mantia, M. Pasta, Characterising lithium-ion electrolytes via operando Raman microspectroscopy, Nat. Commun. 12 (2021) 1–9.
[14] Z. Deng, X. Lin, Z. Huang, J. Meng, Y. Zhong, G. Ma, Y. Zhou, Y. Shen, H. Ding, Y. Huang, Recent progress on advanced imaging techniques for lithium-ion batteries, Adv. Energy Mater. 11 (2021) 1–24.
[15] A.V. Llewellyn, A. Matruglio, D.J.L. Brett, R. Jervis, P.R. Shearing, Using in-situ laboratory and synchrotron-based x-ray diffraction for lithium-ion batteries characterization: a review on recent developments, Condens. Matter 5 (2020) 1–28.
[16] O.J. Borkiewicz, B. Shyam, K.M. Wiaderek, C. Kurtz, P.J. Chupas, K.W. Chapman, The AMPIX electrochemical cell: a versatile apparatus for in situ X-ray scattering and spectroscopic measurements, J. Appl. Crystallogr. 45 (2012) 1261–1269.
[17] O.J. Borkiewicz, K.M. Wiaderek, P.J. Chupas, K.W. Chapman, Best practices for operando battery experiments: influences of X-ray experiment design on observed electrochemical reactivity, J. Phys. Chem. Lett. 6 (2015) 2081–2085.
[18] J. Sottmann, R.H. Regojo, D.S. Wragg, H. Fjellva, S. Margadonnaa, H. Emerich, Versatile electrochemical cell for Li/Na-ion batteries and high-throughput setup for combined operando X-ray diffraction and absorption spectroscopy, J. Appl. Crystallogr. 49 (2016) 1972–1981.
[19] J. Sottmann, V. Pralong, N. Barrier, C. Martin, An electrochemical cell for operando bench-top X-ray diffraction, J. Appl. Crystallogr. 52 (2019) 485–490.
[20] O. Sendetskyi, M. Salomons, P. Mendez, M. Fleischauer, ConFlat cell for operando electrochemical X-ray studies of lithium-ion battery materials in commercially relevant conditions, J. Appl. Crystallogr. 54 (2021) 1416–1423.
[21] O. Gustafsson, A. Schökel, W.R. Brant, Design and operation of an operando synchrotron diffraction cell enabling fast cycling of battery materials, Batter. Supercaps 4 (2021) 1599–1604.
[22] L. Su, P. Choi, B.S. Parimalam, S. Litster, B. Reeja-Jayan, Designing reliable electrochemical cells for operando lithium-ion battery study, MethodsX 8 (2021), 101562.
[23] M. Morcrette, M. Morcrette, Y. Chabre, G. Vaughan, G. Amatucci, J.B. Leriche, S. Patoux, C. Masquelier, J.M. Tarascon, In situ X-ray diffraction techniques as a powerful tool to study battery electrode materials, Electrochim. Acta 47 (2002) 3137–3149.
[24] J.B. Leriche, S. Hamelet, J. Shu, M. Morcrette, C. Masquelier, G. Ouvrard, M. Zerrouki, P. Soudan, S. Belin, E. Elkaïm, F. Baudelet, An electrochemical cell for operando study of lithium batteries using synchrotron radiation, J. Electrochem. Soc. 157 (2010) A606.
[25] M. Bianchini, J.B. Leriche, J.L. Laborier, L. Gendrin, E. Suard, L. Croguennec, C. Masquelier, A new null matrix electrochemical cell for Rietveld refinements of in-situ or operando neutron powder diffraction data, J. Electrochem. Soc. 160 (2013) A2176–A2183.
[26] S. Park, Z. Wang, Z. Deng, I. Moog, P. Canepa, F. Fauth, D. Carlier, L. Croguennec, C. Masquelier, J.N. Chotard, Crystal structure of $Na_2V_2(PO_4)_3$, an intriguing phase spotted in the $Na_3V_2(PO_4)_3$-$Na_1V_2(PO_4)_3$ system, Chem. Mater. 34 (2022) 451–462.
[27] M.F. Talbott, G.S. Springer, L.A. Berglund, The effects of crystallinity on the mechanical properties of PEEK polymer and graphite fiber reinforced PEEK, J. Compos. Mater. 21 (1987) 1056–1081.
[28] TOPAS V6, Bruker-AXS GmbH, Karlsruhe, Germany, 2016. https://www.bruker.com/en/products-and-solutions/diffractometers-and-scattering-systems/x-ray-diffractometers/diffrac-suite-software/diffrac-topas.html.
[29] M.R. Rowles, C.E. Buckley, Aberration corrections for non-Bragg–Brentano diffraction geometries, J. Appl. Crystallogr. 50 (2017) 240–251.
[30] W. Li, J.N. Reimers, J.R. Dahn, In situ x-ray diffraction and electrochemical studies of $Li_{1-x}NiO_2$, Solid State Ionics 67 (1993) 123–130.
[31] H. Ryu, K. Park, C.S. Yoon, Y. Sun, Capacity fading of Ni- cat h- odes for high energy density lithium- lithium - ion batteries : bulk or surface degradation, Chem. Mater. 2 (2018) 1–9.
[32] C.D. Quilty, D.C. Bock, S. Yan, K.J. Takeuchi, E.S. Takeuchi, A.C. Marschilok, Probing sources of capacity fade in $LiNi_{0.6}Mn_{0.2}Co_{0.2}O_2$ (NMC622): an operando

XRD study of Li/NMC622 batteries during extended cycling, J. Phys. Chem. C 124 (2020) 8119–8128.
[33] D.H.S. Tan, A. Banerjee, Z. Chen, Y.S. Meng, From nanoscale interface characterization to sustainable energy storage using all-solid-state batteries, Nat. Nanotechnol. 15 (2020) 170–180.
[34] M.M. Doeff, R.J. Clément, P. Canepa, Solid electrolytes in the spotlight, Chem. Mater. 34 (2022) 463–467.
[35] R.P. Rao, S. Adams, Studies of lithium argyrodite solid electrolytes for all-solid-state batteries, Phys. Status Solidi Appl. Mater. Sci. 208 (2011) 1804–1807.
[36] S. Boulineau, J.M. Tarascon, J.B. Leriche, V. Viallet, Electrochemical properties of all-solid-state lithium secondary batteries using Li-argyrodite Li_6PS_5Cl as solid electrolyte, Solid State Ionics 242 (2013) 45–48.
[37] S. Wang, M. Tang, Q. Zhang, B. Li, S. Ohno, F. Walther, R. Pan, X. Xu, C. Xin, W. Zhang, L. Li, Y. Shen, F.H. Richter, J. Janek, C.W. Nan, Lithium argyrodite as solid electrolyte and cathode precursor for solid-state batteries with long cycle life, Adv. Energy Mater. 11 (2021) 1–10.
[38] J. Zhang, C. Zheng, J. Lou, Y. Xia, C. Liang, H. Huang, Y. Gan, X. Tao, W. Zhang, Poly(ethylene oxide) reinforced $Li_6PS_5C_l$ composite solid electrolyte for all-solid-state lithium battery: enhanced electrochemical performance, mechanical property and interfacial stability, J. Power Sources 412 (2019) 78–85.
[39] C. Yu, Y. Li, M. Willans, Y. Zhao, K.R. Adair, F. Zhao, W. Li, S. Deng, J. Liang, M. N. Banis, R. Li, H. Huang, L. Zhang, R. Yang, S. Lu, Y. Huang, X. Sun, Superionic conductivity in lithium argyrodite solid-state electrolyte by controlled Cl-doping, Nano Energy 69 (2020), 104396.
[40] L. Ye, X. Li, A dynamic stability design strategy for lithium metal solid state batteries, Nature 593 (2021) 218–222.
[41] Y. Xiang, X. Li, Y. Cheng, X. Sun, Y. Yang, Advanced characterization techniques for solid state lithium battery research, Mater. Today 36 (2020) 139–157.
[42] A. Jena, Z. Tong, B. Bazri, K. Iputera, H. Chang, S.F. Hu, R.S. Liu, In situ/operando methods of characterizing all-solid-state Li-ion batteries: understanding Li-ion transport during cycle, J. Phys. Chem. C 125 (2021) 16921–16937.
[43] T. Asano, A. Sakai, S. Ouchi, M. Sakaida, A. Miyazaki, S. Hasegawa, Solid halide electrolytes with high lithium-ion conductivity for application in 4 V class bulk-type All-solid-state batteries, Adv. Mater. 30 (2018) 1–7.
[44] T. Bartsch, A.Y. Kim, F. Strauss, L.D. Biasi, J.H. Teo, J. Janek, P. Hartmannad, T. Brezesinski, Indirect state-of-charge determination of all-solid-state battery cells by X-ray diffraction, Chem. Commun. 55 (2019) 11223–11226.
[45] A.E. Kharbachi, J. Wind, A. Ruud, A.B. Høgset, M.M. Nygård, J. Zhang, M.H. Sørby, S. Kim, F. Cuevas, S. Orimo, M. Fichtner, M. Latroche, H. Fjellvågc, B.C. Haubacka, Pseudo-ternary $LiBH_4{\cdot}LiCl{\cdot}P_2S_5$system as structurally disordered bulk electrolyte for all-solid-state lithium batteries, Phys. Chem. Chem. Phys. 22 (2020) 13872–13879.
[46] S. Kaboli, H. Demers, A. Paolella, A. Darwiche, M. Dontigny, D. Clément, A. Guerfi, M.L. Trudeau, J.B. Goodenough, K. Zaghib, Behavior of solid electrolyte in Li-polymer battery with NMC cathode via in-situ scanning electron microscopy, Nano Lett. 20 (2020) 1607–1613.
[47] W. Li, S. Lee, A. Manthiram, High-nickel nma: a cobalt-free alternative to NMC and nca cathodes for lithium-ion batteries, Adv. Mater. 32 (2020).